INTERNATIONAL JOURNAL OF INTEGRATED ENGINEERING
ISSN: 2229-838X e-ISSN: 2600-7916

IJIE

Vol. 17 No. 6 (2025) 71-83
https://publisher.uthm.edu.my/ojs/index.php/ijie

Electromagnetic Simulation of Metamaterial Lens Antenna with Negative Refractive Index at 28GHz

Mohamed Farouk Al Ghifarry[1], Kamilia Kamardin[2]*, Yoshihide Yamada[2], Izni Husna Idris[3]

[1] *Department of Electronic Systems Engineering, Malaysia-Japan International Institute of Technology (MJIIT), Universiti Teknologi Malaysia, Kuala Lumpur, MALAYSIA*
[2] *Wireless Communication Centre, Universiti Teknologi Malaysia, Kuala Lumpur, MALAYSIA*
[3] *Department of Electric and Electronic, Faculty of Engineering, Universiti Pertahanan Nasional Malaysia, Kuala Lumpur, MALAYSIA*

*Corresponding Author: kamilia@utm.my
DOI: https://doi.org/10.30880/ijie.2025.17.06.006

Article Info

Received: 26 March 2025
Accepted: 28 October 2025
Available online: 30 December 2025

Keywords

Negative lens, negative refractive index, focal region ray tracing, lens antenna, electromagnetic simulation

Abstract

Lens antennas are widely used to achieve multi-beam radiation patterns. When designed with negative refractive index (NRI) materials, these patterns can be enhanced due to reduced lens thickness and improved focusing properties. However, accurately simulating NRI-based lens antennas remains a challenge, as many electromagnetic (EM) solvers do not fully support negative material parameters. This paper presents a step-by-step methodology for modeling and analyzing NRI lens antennas using ANSYS HFSS, a finite element method (FEM)-based simulator. The simulation procedure covers material assignment, boundary condition selection, and setup for near- and far-field calculations. Quantitative results demonstrate that the 100 mm and 200 mm NRI lenses achieve gains of 26.6 dBi and 32.98 dBi, with beamwidths of 7.75° and 3.66°, respectively, and radiation efficiencies of approximately 70%. These results closely agree with theoretical predictions, validating HFSS as a reliable tool for NRI lens antenna simulation and providing a practical reference for future lens design studies.

1. Introduction

In 5G mobile communication systems, base station antennas require multi-beam radiation patterns [1],[2]. Lens antennas are well known for their ability to achieve multibeam patterns efficiently [3],[4],[5]. Traditional lens antennas, which use dielectric materials, typically feature a convex surface structure [6],[7]. However, when a negative refractive index (NRI) material is used, the lens surface takes on a concave shape instead. This structural change significantly reduces lens thickness compared to convex designs [8],[9]. Recent studies have explored the design and optimization of such lenses using advanced simulation techniques, particularly in the context of 5G and mm Wave applications [10],[11]. A thinner lens is expected to enhance multi-beam radiation performance, making NRI lenses an appealing option.

The same design equations applied to positive refractive index lenses can also be used NRI lenses. However, accurately simulating their radiation patterns using commercial electromagnetic software can be challenging, as only a few simulators support NRI materials. In this case HFSS is utilized to tackle the challenge [12]. Other recent works have demonstrated the effectiveness of HFSS in modeling NRI lens structures [13].

This paper presents electromagnetic simulation examples of an NRI lens using HFSS. First, the lens structure formation process and parameter settings for NRI materials are explained. The distribution of the electric field on the aperture plane and the far and near fields are the important electromagnetic outcomes. Lastly, the accuracy of the simulation findings is assessed by comparing them with theoretical calculations.

2. Lens Structure

Fig. 1 shows the antenna structure of an NRI lens. With this design, a feed horn behind the lens illuminates the lens. The ray tracing approach is used to design the lens surface. The feed horn's rays bend and align themselves with the horizontal axis because of refractive action at the lens surface. The fundamental equations for determining lens shapes are the equality condition of electrical path length shown as equation (1).

$$F - |n|T = r - |n|(F + T - r\cos\theta) \tag{1}$$

Then the equation is simplified into equation (2).

$$r\,(-|n|\cos\theta - 1) = F\,(-|n| - 1) \tag{2}$$

Equation (3) determines the shape of the lens surface [7].

$$r = \frac{F(-|n| - 1)}{-|n|\cos\theta - 1} \tag{3}$$

F represents focal distance, and n denotes the refractive index, which in this case is negative.

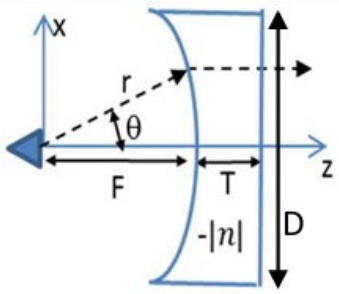

Fig. 1 *Shape of NRI lens*

The structural specifications are outlined in Table 1. An operating frequency of 28 GHz is selected, considering the millimeter-wave range used in 5G communications. To simplify calculations, antenna diameters of 100 mm and 200 mm are chosen.

Table 1 *Parameter of NRI lens*

Parameter	Value	Value
Antenna diameter, D	10 cm	20 cm
Antenna radius, R	5 cm	10 cm
Focal length, F	8 cm	12 cm
Lens Thickness, T	0.6 cm	1 cm
Maximum angle, θ_M	25°	43°
Refractive index, n	√-2.17	-2
Permittivity, ε	-2.17	-4
Permeability, μ	-1	-1
Frequency, *f*	28 GHz	28 GHz
Wavelength, λ	1.07 cm	1.07 cm

Int. Journal of Integrated Engineering Vol. 17 No. 6 (2025) p. 71-83

3. Simulator Explanation

A flowchart is provided to illustrate the simulation steps for the NRI lens antenna, as shown in Fig. 2 below.

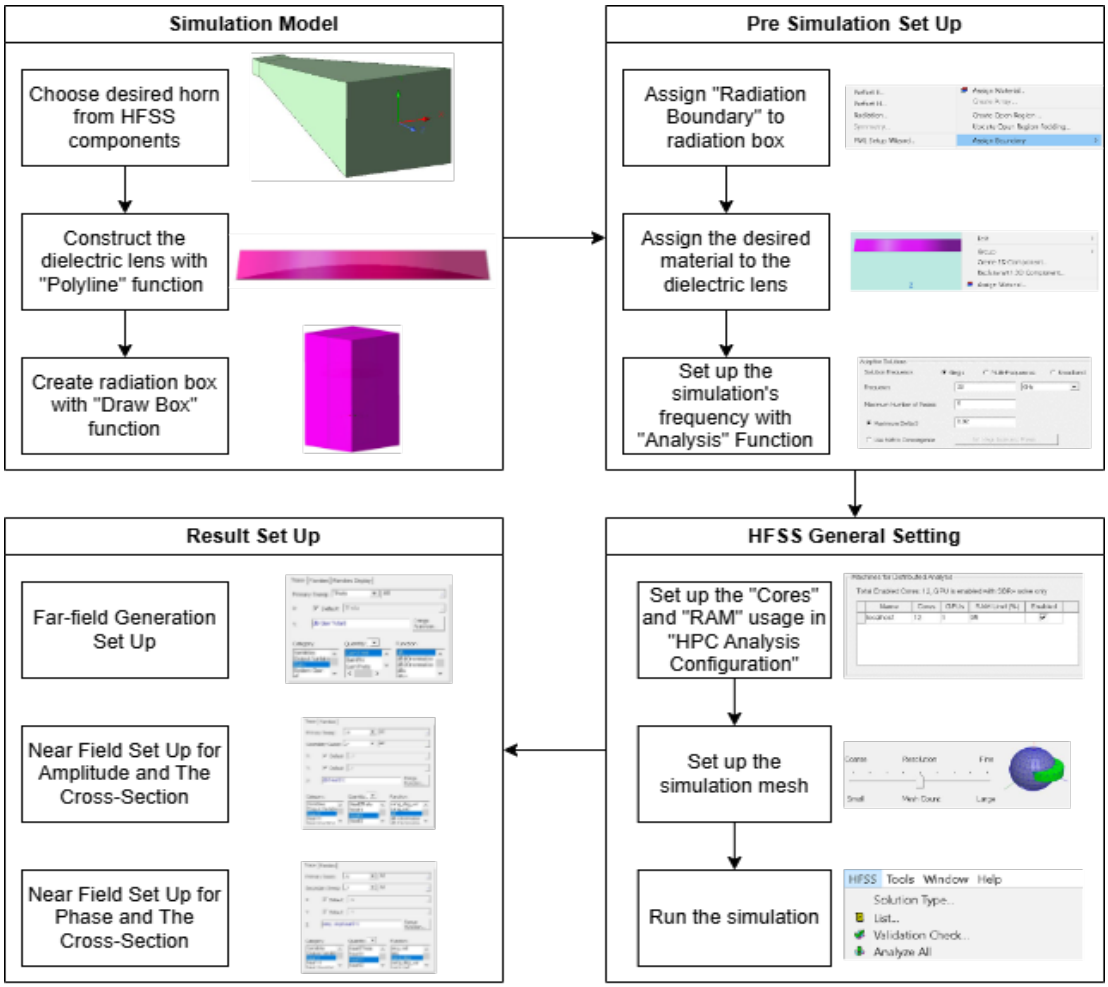

Fig. 2 *Step by step on how to operate HFSS*

3.1 Lens Geometry and Setup

The simulation setup consists of a horn antenna, an NRI lens, and a radiation box, as illustrated in Fig. 3 for the 100 mm lens. The horn can be created from the "HFSS component" database found in the "Antenna" and "Waveguide" categories by selecting the "Horn Pyramidal WR90 DM" option. Its specifications can be modified to suit specific requirements. To guarantee precision in the lens's design, it is highly recommended to use the "polyline" tool. The "Draw box" or "Create region" functions are utilized to generate the radiation box, with flexibility to adjust its dimensions as required.

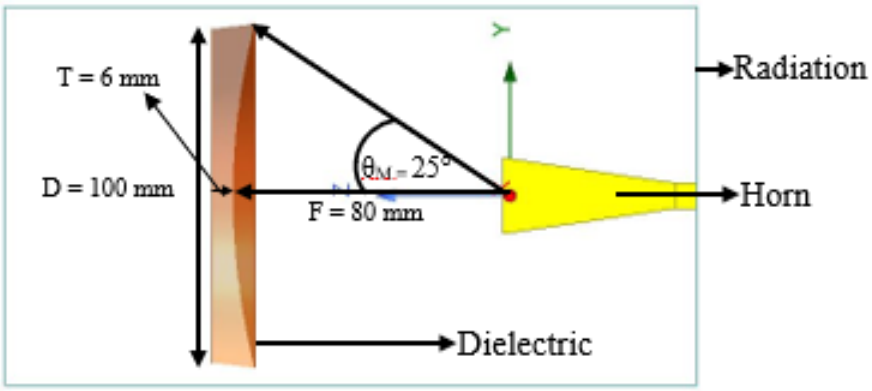

Fig. 3 *Air box radiation boundary for 100mm lens*

To expedite the simulation time for larger geometries, such as the 200mm as shown in Fig. 4, the Finite Element–Boundary Integral (FE-BI) boundary condition is used instead of a traditional radiation boundary. Unlike standard boundaries, which are limited to a box shape, the FE-BI boundary consists of two separate boundaries, one for the lens and one for the horn. This flexibility allows it to conform to the shape of the lens and horn, optimizing the simulation domain. The FE-BI method efficiently couples the Finite Element Method (FEM) inside the simulation domain with the Boundary Integral (BI) method on the outer region, reducing the need for extensive meshing and preventing unwanted reflections. As a result, this approach significantly reduces both memory usage and computation time while maintaining accuracy in the simulation.

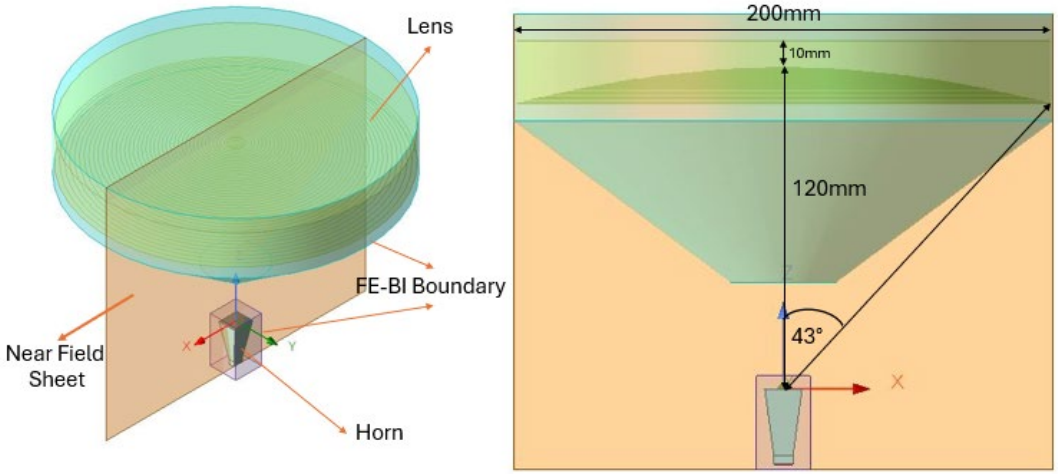

Fig. 4 *FE-BI boundary condition for 200mm lens*

3.2 Material Setting

To assign the appropriate material to the NRI lens, the lens must be right clicked, followed by selecting the “Assign Material” option. If the desired material with the specific properties is not available in the simulator, a new material must be added. The "View/Edit Material" option is used to change the material's properties, and the "Add Material" feature makes this procedure easier. As seen in Fig. 6, the relative permittivity and permeability for the 100 mm lens are adjusted to -2.17 and -1, respectively, and Fig. 7 shows -4 and -1 are set for the 200 mm lens.

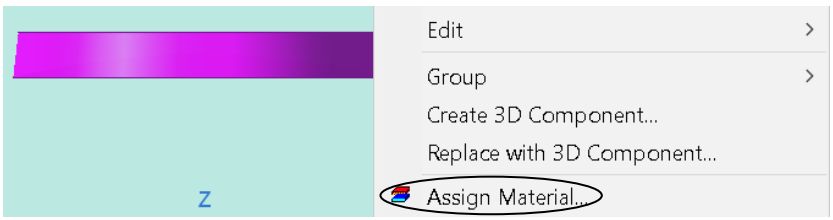

Fig. 5 *Material assigning*

Int. Journal of Integrated Engineering Vol. 17 No. 6 (2025) p. 71-83

Properties of the Material

	Name	Type	Value
	Relative Permittivity	Simple	-2.17
	Relative Permeability	Simple	-1

Fig. 6 *Set material for 100mm lens*

Properties of the Material

	Name	Type	Value
	Relative Permittivity	Simple	-4
	Relative Permeability	Simple	-1

Fig. 7 *Set material for 200mm lens*

3.3 Simulator General Setting

Before initiating the simulation, it is necessary to adjust key configuration settings, such as RAM limit and used CPU cores through the "HPC Analysis Configuration" section in the "Driven Solution Setup" window. As seen in Fig. 8, the RAM limit was raised from 90% to 95% to maximize simulation speed, and the number of CPU cores was adjusted based on the CPU's capabilities, ranging from 4 to 12 cores. Find out how many CPU cores are being used by going to the "Performance" section of the "Windows Task Manager."

Machines for Distributed Analysis

Total Enabled Cores: 12, GPU is enabled with SBR+ solve only

	Name	Cores	GPUs	RAM Limit (%)	Enabled
	localhost	12	1	95	✔

Fig. 8 *Changing number of RAM and CPU cores*

The choice of meshing methodology plays a crucial role in determining the simulation's time. As shown on Fig. 9, the mesh size can be adjusted to achieve an equal ratio between coarse and fine meshes. A coarse mesh leads to faster simulation times but with reduced accuracy. On the other hand, fine mesh improves accuracy at the cost of longer simulation durations. To maximize simulation speed and result accuracy, a standard mesh size was chosen in this instance.

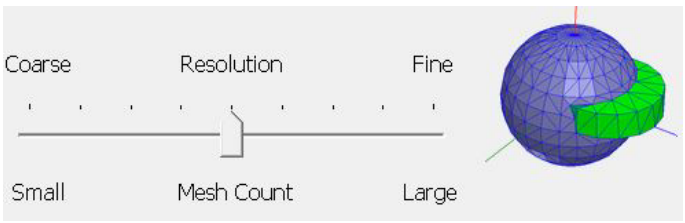

Fig. 9 *Meshing slider*

3.4 Set Up for Far Field

To obtain the far field results, go to the "Project Manager," pick on the "Results" section, and select "Create Far Field Report." Choose the "Rectangular Plot" option. Once the window appears, configure the settings by selecting "Gain" as the "Category", "GainTotal" as the "Quantity", and "dB" as the "Function", as shown in Fig. 10. Finally, click "New Report" to obtain the results.

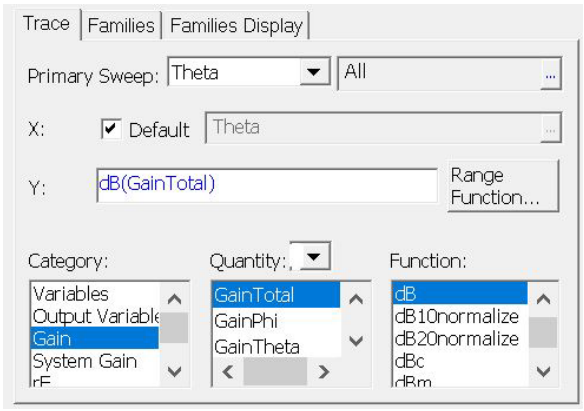

Fig. 10 *Set up for gain (far field)*

3.5 Set Up for Near Field

The procedure to determine the amplitude and phase for the near field is outlined in Fig. 11. In the "Project Manager," pick on "Results" to access both near field data. To plot the amplitude, choose "Create Near Field Report," followed by selecting "Rectangular Contour Plot". The cross-sectional plot can be created by choosing "Create Near Field Report" and then "Rectangular Plot." Put "Near E" as the "Category," "NearEY" as the "Quantity," and "dB" as the function in new display. Click "New Report" to produce the cross-sectional and amplitude results. Repeat the same procedure, replacing "dB" with "Cang_Deg," and leave "Near E" and "NearEY" as the "Category" and "Quantity," respectively, to obtain the phase and its cross-section.

Fig. 11 *Set up for (a) Amplitude; (b)and Cross-section; (c) Phase; and (d) Cross-section*

4. Simulation Results

To guarantee that the simulation runs smoothly and without errors, it's essential to change several parameters within the simulator. The relevant simulation parameters are listed in Table 2.

Int. Journal of Integrated Engineering Vol. 17 No. 6 (2025) p. 71-83

Table 2 *NRI lens simulation parameter*

Parameter	Details	
Electromagnetic Simulator	ANSYS HFSS	
Simulation Method	FEM	
CPU	Intel Xeon CPU E5-2683 v4	
Speed	2.10 GHz	
GPU	NVDIA Quadro M5000	
RAM	524 GB	
Diameter Lens, mm	100 mm	200 mm
Boundary Type	Air Box Radiation Boundary	Finite Element Boundary Integral
Mesh Used	Moderate Type	
Time Used	4H: 20M: 30S	1H: 16M: 4S
Memory Used	85.5 GB	73 GB
Result	Success	Success

4.1 Parameter and Radiation Characteristic of Horn

A pyramidal horn antenna, designed to operate at 28 GHz, serves as the feed radiator, directing electromagnetic waves in a specific direction. The horn's geometry is depicted in Fig. 12, with aperture dimensions of 7.112 mm × 3.556 mm, and its parameters are listed in Table 3. This antenna produces a unidirectional radiation pattern, achieving a gain of 16.79 dBi. The resulting radiation patterns, illustrated in Fig. 13, show an E-Plane beamwidth of 51.53°.

Table 3 *Parameter of horn*

Variable	Quantity
Waveguide size, mm (Ww × Lw × Hw)	7.112 × 3.556 × 3.0
Horn size, mm (Wh × Lh × Hh)	25.0 × 22.0 × 53.0
Gain, dBi	16.79
Material	PEC

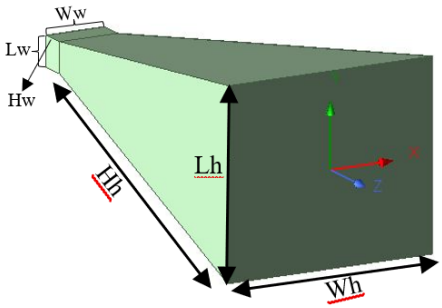

Fig. 12 *Horn structure*

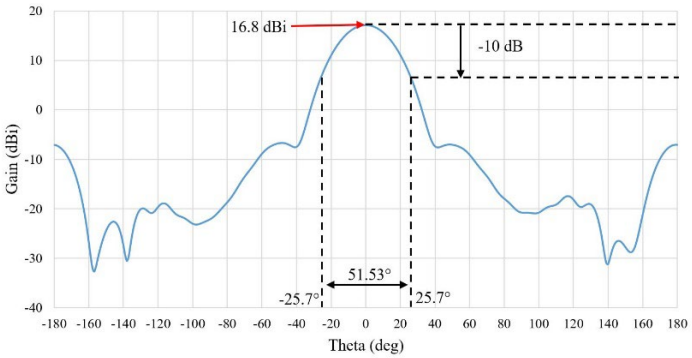

Fig. 13 *Horn radiation pattern*

4.2 Near Field Distribution

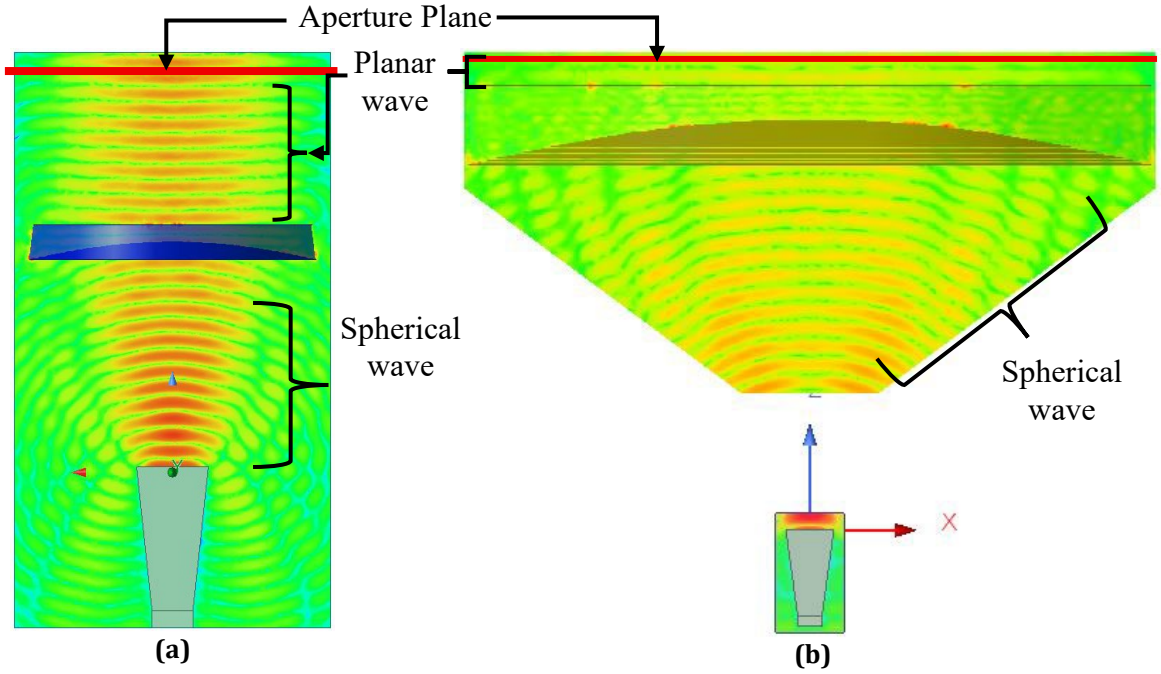

Fig. 14 *NRI near field result of (a) Air box radiation boundary; and (b) FE-BI boundary*

The suggested model's dependability is assessed by near-field distribution simulations, with a focus on the electric field distributions at 28 GHz. Horn antennas typically generate cylindrical or spherical waves which come from the radiation pattern. When these waves enter the antenna lens, the rays refract according to Snell's law. After the spherical wave from the feed horn goes through the lens, the wave transforms into a planar wave, where the rays become nearly parallel. After passing through the lenses, these waveforms evolve into planar shapes and are evenly distributed, as illustrated in Fig 14. (a) and Fig 14. (b). However, distortion happens at both Fig 14. (b) and 14. (b). This may happen due to the interaction of horn radiation pattern and lens surface which may cause reflection. This results in less ideal uniformity of the spherical wave.

4.3 Aperture Field Distribution

The electric field amplitude distribution for the 100 mm and 200 mm lenses, obtained from near-field calculations, is illustrated in Fig. 15(a) and 15(b). The results show a generally symmetrical pattern; however, noticeable ripples appear near the circumference of the aperture plane for both lens sizes, particularly at the 0° horn antenna position. These ripples are likely a byproduct of distortions in the feed horn radiation pattern, which deviates from the ideal uniform feed behavior. The amplitude cross-section demonstrates a tapered profile, gradually decreasing from the lens center toward the edge, with edge levels of approximately −24 dB and −20 dB for the 100 mm and 200 mm lenses, respectively.

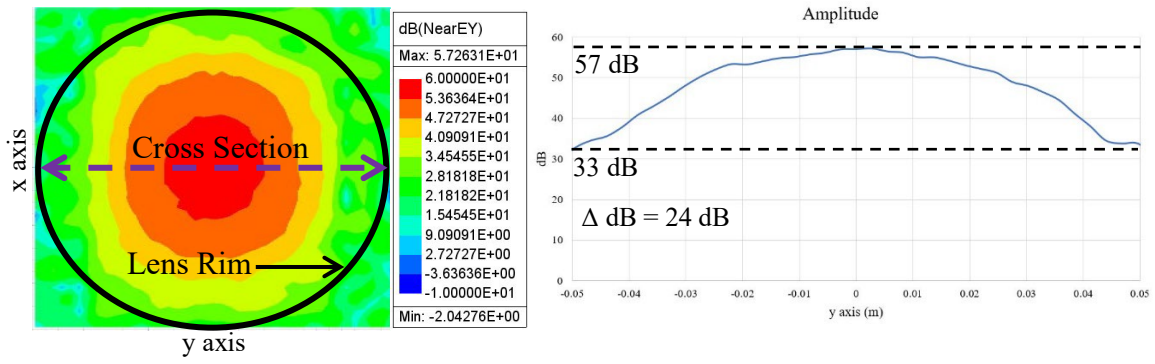

(a)

Int. Journal of Integrated Engineering Vol. 17 No. 6 (2025) p. 71-83

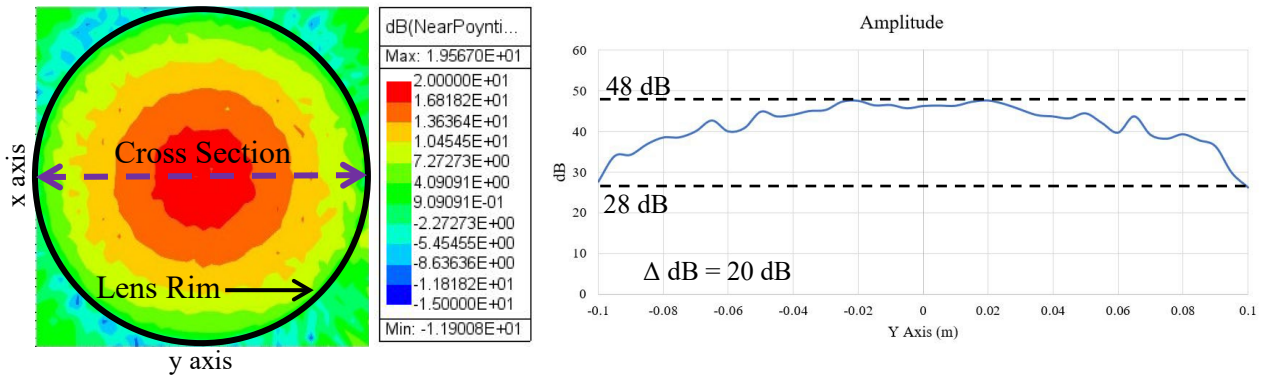

(b)

Fig. 15 *(a) 100 mm lens amplitude aperture distribution & cross section; and (b) 200 mm lens amplitude aperture distribution & cross section*

The phase distribution results, shown in Fig. 16(a) and 16(b), exhibit relatively stable values along the central axis of the aperture; however, reduced uniformity is observed near the circumference. This irregularity may also be attributed to deformations in the feed horn radiation pattern, as evident in Fig. 14, where the feed deviates from its ideal profile. Such non-uniform phase behavior, combined with the observed amplitude ripples, indicates that the feed alignment and lens configuration influence the overall aperture field distribution.

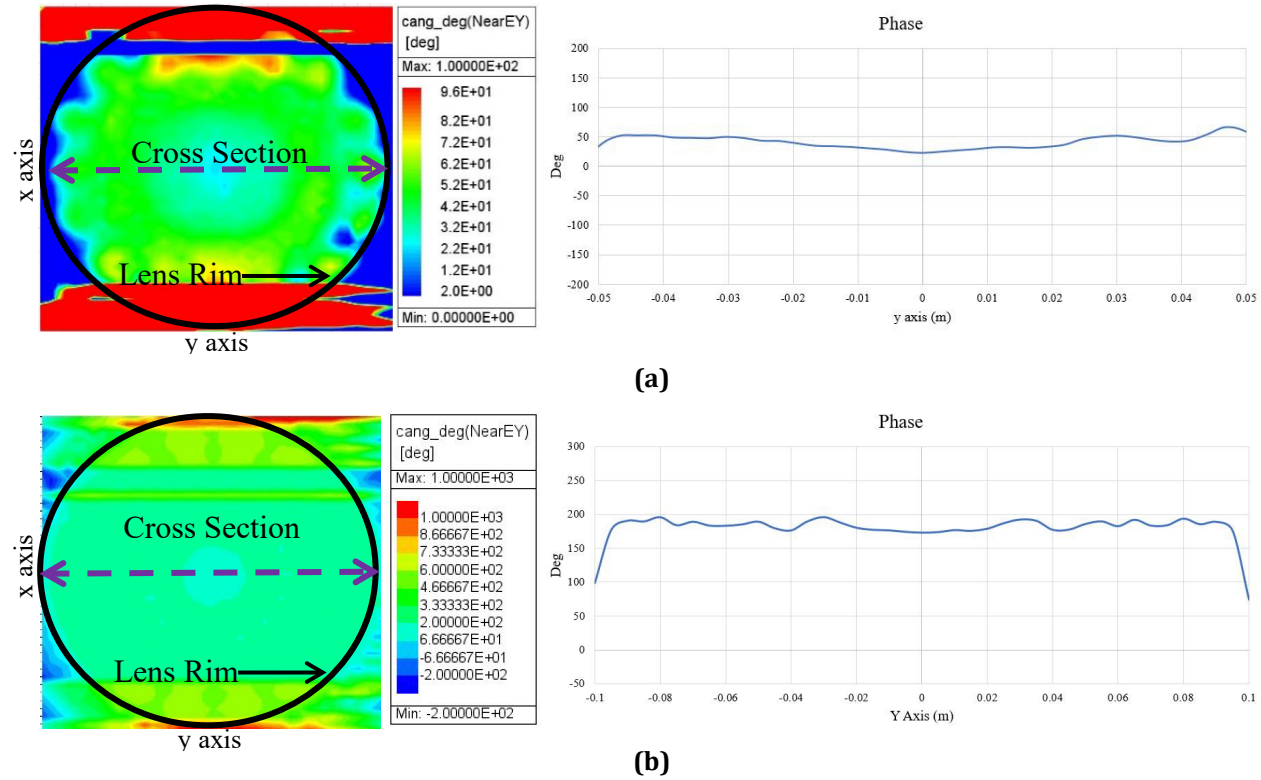

(a)

(b)

Fig. 16 *(a) 100 mm lens phase aperture distribution & cross section; and (b) 200 mm lens phase aperture distribution & cross section*

Future improvements can be explored to minimize the distorted aperture field distribution observed in both amplitude and phase. Potential optimization efforts include adjusting the lens focal length-to-diameter (f/D) ratio, modifying the lens geometry, or incorporating a matching layer. Implementing these enhancements in future designs could lead to a smoother aperture field distribution, reduced edge ripples, and improved overall lens radiation performance.

4.4 Radiation Pattern

The radiation pattern for the 100mm lens is shown in Fig. 17, with a gain of 26.60 dBi and a beamwidth of 7.75°.

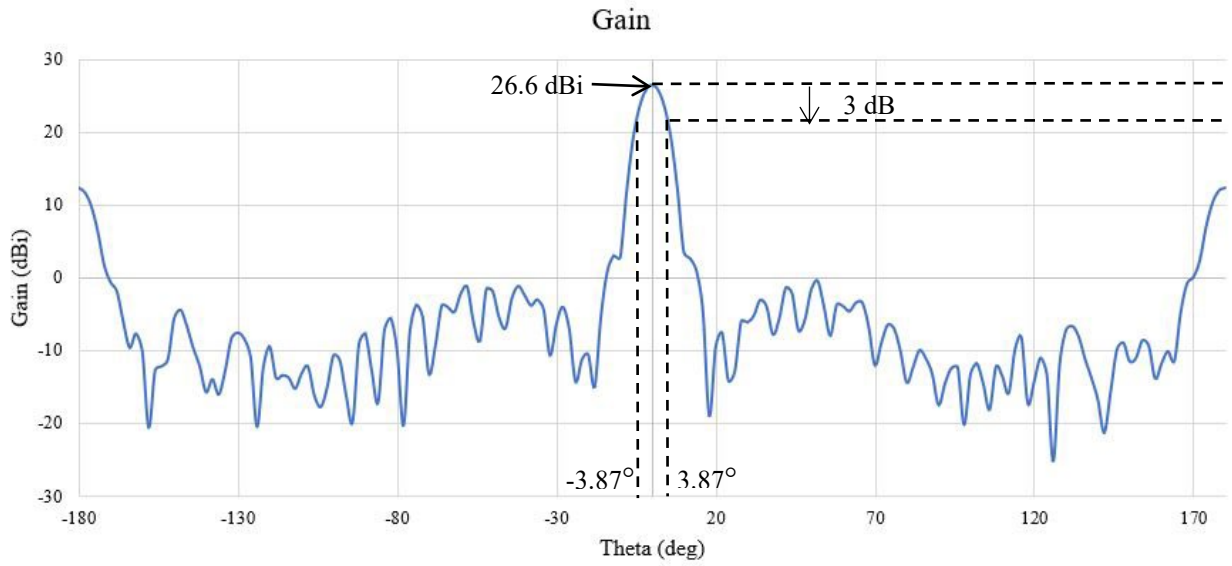

Fig. 17 *100mm lens gain and radiation pattern*

To validate the simulation result, theoretical calculation of gain is calculated as derived in equation (4)

$$G = (\frac{\pi D}{\lambda})^2 = (\frac{\pi 100}{10.7})^2 = 29.35\ dBi \tag{4}$$

Based on the tapered amplitude in Fig. 15(a), the approximate gain is calculated as follows.

$$\begin{gathered} 10\log 0.75 = -1.25 \\ 29.35\ dBi - 1.25 = 28.1\ dBi \end{gathered} \tag{5}$$

The main beam width is measured at 7.75° with sidelobe level of 27 dB, slightly wider than the theoretical beam width at 7.49° as calculated in equation (6), suggesting excellent beam focusing capability.

$$1.22\frac{\lambda}{D} = 1.22\frac{10.7}{100} = 0.13054rad = 7.49° \tag{6}$$

For the 200mm lens, the radiation pattern is shown in Fig. 18. This lens produces a higher gain of 32.987 dBi and a beamwidth of 3.66°. The comparison of theoretical and simulated results for both 100mm and 200mm lens can be found in Table 4.

Int. Journal of Integrated Engineering Vol. 17 No. 6 (2025) p. 71-83

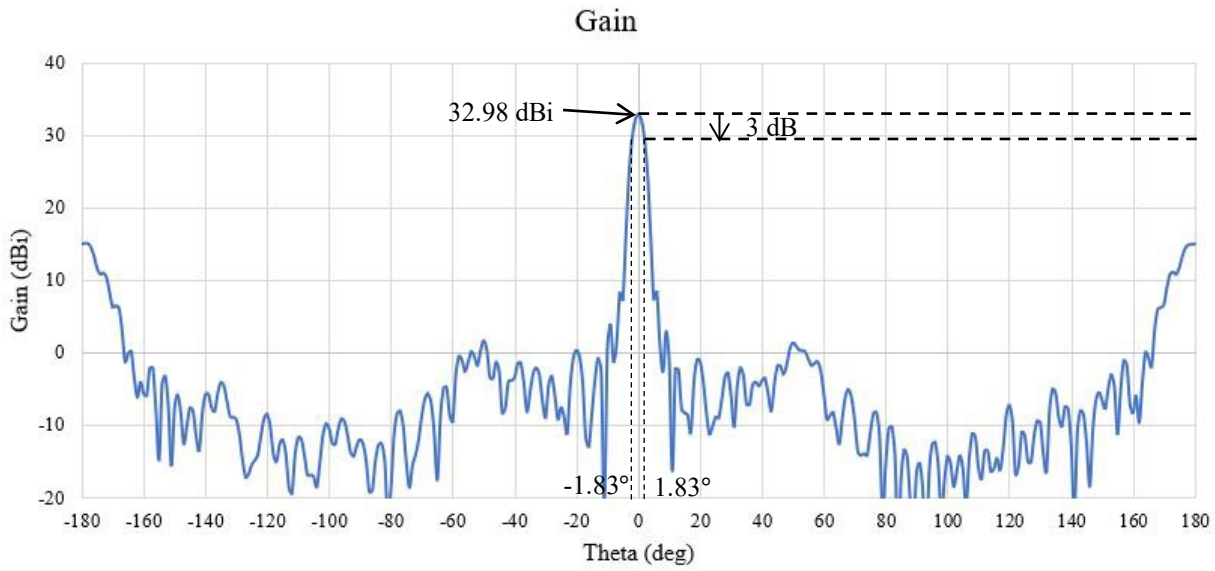

Fig. 18 *200mm lens gain and radiation pattern*

To validate the simulation result, theoretical calculation of gain is calculated as derived in equation (7)

$$G = (\frac{\pi D}{\lambda})^2 = (\frac{\pi 200}{10.7})^2 = 35\ dBi \tag{7}$$

Based on the tapered amplitude in Fig. 15(b), the approximate gain is calculated as follows.

$$\begin{gathered} 10\log 0.75 = -1.25 \\ 35\ dBi - 1.25 = 33.75\ dBi \end{gathered} \tag{8}$$

The main beam width is measured at 3.66° with sidelobe level of 16.22 dB, slightly narrower than the theoretical beam width at 3.74° as calculated in equation (9), suggesting excellent beam focusing capability.

$$1.22\frac{\lambda}{D} = 1.22\frac{10.7}{200} = 0.0653rad = 3.74° \tag{9}$$

Table 4 *100mm and 200mm lens theoretical and simulation comparison*

	100mm lens		200 mm lens	
	Simulation	Calculation	Simulation	Calculation
Beam width, degree	7.75	7.49	3.66	3.74
Sidelobe level, dB	-27.0	-20.0	-16.220	-24.4
Gain, dBi	26.60	29.35	32.987	35

The comparison between simulation and theoretical results shows that HFSS successfully captures the key electromagnetic behavior of the NRI lens antenna. The difference in gain between the simulation and theoretical values (e.g., 26.60 dBi vs. 29.35 dBi) is likely due to wave bending or scattering at the lens edges and minor misalignments in the horn feed positioning. This kind of diffraction is common in practical setups and can cause slight drops in performance compared to ideal calculations. Despite these differences, the beamwidth and sidelobe levels closely match theoretical values, validating the effectiveness of the HFSS model. The 200 mm lens exhibits better focusing and directivity, which aligns with its larger aperture and reduced divergence. These findings confirm the NRI lens' potential to enhance gain and narrow beamwidths, essential for 5G applications.

5. Conclusions

This study demonstrated the feasibility of using ANSYS HFSS to accurately simulate a negative refractive index (NRI) lens antenna, overcoming limitations faced by other electromagnetic solvers. A step-by-step approach was outlined, covering lens geometry creation, material assignment, boundary condition selection, and field analysis, serving as a practical guide for beginners working with NRI lenses. The simulation results showed that both the 100 mm and 200 mm lenses successfully converted spherical feed waves into plane waves, producing high-gain and narrow-beam radiation patterns of 26.6 dBi (7.75°) and 32.98 dBi (3.66°), respectively. These results closely matched theoretical calculation, validating the simulation methodology and achieving an overall radiation efficiency of approximately 70%. Minor distortions observed in aperture field distributions were attributed to irregular horn radiation patterns, suggesting potential improvements through feed alignment, f/D optimization, or the addition of matching layers. Overall, this work confirms that HFSS is a reliable tool for modeling NRI lens antennas and provides a foundation for future studies on multibeam optimization and advanced lens designs for 5G applications.

Acknowledgement

The author would like to thank the Communication System and Networks (CSN) Research Group, MJIIT, UTM Kuala Lumpur. This work was supported by the Ministry of Higher Education (MoHE), Universiti Teknologi Malaysia (UTM) through the UTM Fundamental Research Grant Scheme (Q.K130000.3843.22H39).

Conflict of Interest

Authors declare that there is no conflict of interest regarding the publication of the paper.

Author Contribution

The authors confirm contribution to the paper as follows: ***study conception and design:*** *Mohamed Farouk Al Ghifary, Kamilia Kamardin, Yoshihide Yamada, and Izni Husna Idris;* ***data collection:*** *Mohamed Farouk Al Ghifary, and Izni Husna Idris;* ***analysis and interpretation of results:*** *Mohamed Farouk Al Ghifary, Kamilia Kamardin, and Yoshihide Yamada;* ***draft manuscript preparation:*** *Mohamed Farouk Al Ghifary, Kamilia Kamardin, Yoshihide Yamada, and Izni Husna Idris. All authors reviewed the results and approved the final version of the manuscript.*

References

[1] Dardari D et al 2017 5G Networks: An Overview of Massive MIMO, mmWave, and Non-Orthogonal Multiple Access IEEE J. Sel. Areas Commun. 35 1201-1215

[2] W. Hong et al 2017 Multibeam Antenna Technologies for 5G Wireless Communications in IEEE Transactions on Antennas and Propagation, vol. 65, no. 12, pp. 6231 - 6249.

[3] Y. T. Lo and S. W. Lee, Antenna Handbook: Theory, Applications, and Design, Van Nostrand Reinhold, 1988, pp. 15-61.

[4] M. Muhsin, K. Kamardin, Y. Yamada, et al 2024 Best Feed Positions and Radiation Patterns of Typical Multibeam Dielectric Lens Antenna, IEEE Access.

[5] Itoh T et al 2012 Lens and Reflector Antennas for Adaptive Wireless Communications *Proc. IEEE* **100** 2341-2352

[6] S. Silver, *Microwave Antenna Theory and Design*, reprint ed., The Institution of Engineering and Technology, 1984. (New York, NY, USA: McGraw-Hill)

[7] Y. Yamada, M. Muhsin, I. H. Idris, K. Kamardin, Y. Sugimoto and K. Sakakibara 2024 Lens Shape Equations for Positive and Negative Refractive Index IEEE Conference on Antenna Measurements and Applications (CAMA), Da Nang, Vietnam, pp. 1-4.

[8] I. H. Idris, M. F. Al-Ghifarry, K. Kamardin, Y. Yamada and M. T. Jusoh 2024 Multibeam Radiation Patterns of Positive and Negative Index Lens Antennas International Symposium on Antennas and Propagation (ISAP), Incheon, Korea, Republic of, pp. 1-2.

[9] Pendry J B 2000 Negative Refraction Makes a Perfect Lens *Phys. Rev. Lett.* **85** 3966-3969

[10] J. Jin 2014 The Finite Element Method in Electromagnetics, 3rd ed., Wiley.

[11] Lo Y 1993 Antenna Handbook: Antenna Fundamentals and Mathematical Techniques. *Springer Science & Business Media*.

Int. Journal of Integrated Engineering Vol. 17 No. 6 (2025) p. 71-83

[12] Phan, V. H., Nguyen, Q. D., Yoshihide, Y., et al 2020 Parametric Analysis of Negative and Positive Refractive Index Lens Antenna by ANSYS HFSS, International Journal of Antennas and Propagation, vol. 2020, Article ID 9128921, 8 pages. doi: 10.1155/2020/9128921

[13] Phan, V. H., Nguyen, Q. D., Yoshihide, Y., 2021Negative Refractive Index-Shaped Lens Antenna with Straight Line Condition for Wide Angle Beam Scanning, Journal of Electromagnetic Waves and Applications, vol. 35, no. 15, pp. 2031–2043, 2021. doi: 10.1080/09205071.2021.1990801